International Journal of Heat and Mass Transfer 195 (2022) 123143

Contents lists available at ScienceDirect

International Journal of Heat and Mass Transfer

journal homepage: www.elsevier.com/locate/hmt

# Heat transfer characteristics of a high-pressure turbine under combined distorted hot-streak and residual swirl: an unsteady computational study

Zakaria Mansouri*, Richard Jefferson-Loveday

*Gas Turbines and Transmissions Research Centre (G2TRC), Faculty of Engineering, University of Nottingham, Nottingham NG7 2RD, United Kingdom*

ARTICLE INFO

*Article history:*
Received 17 February 2022
Revised 8 June 2022
Accepted 11 June 2022

*Keywords:*
Temperature non-uniformity
Heat transfer
Turbine stage
Swirling flow
Numerical simulation

ABSTRACT

In new generation aero-engines, lean-burn combustors are equipped with swirl injectors in order to reduce pollutant emissions. At the exit of these combustors, the flow is dominated by temperature non-uniformity (hot-streak) and residual swirl. Available research has focused mainly on the isolated effects of the residual swirl only or the hot-streak only on the aerodynamic performance or thermal performance of the high-pressure turbine (HPT). Only few studies investigated the combined swirl and hot-streak on the aerothermal performance of the HPT using either idealized uniform or rounded hot-streak topologies. Realistic hot-streaks generated from lean burn combustors have more complex topologies that involves distortions. The present study investigates the effects of residual swirl and distorted hot-streak simultaneously on a first stage of a HPT. Other hot-streak types, uniform and rounded, have been also investigated with and without swirl to perform comparisons with the distorted hot-streak. Unsteady Reynolds-averaged Navier–Stokes (URANS) computations have been conducted to assess the aerothermal performance of a HPT under the influence of different hot-streaks. Results revealed that all hot-streaks without swirl were almost preserved as transported through the vane and altered as transported through the rotor due to the secondary flows. Under the residual swirl, all hot-streaks were remarkably altered at the vane exit and deformed more at the rotor exit. The uniform hot-streak was homogenised through the rotor and the rounded and distorted hot-streaks were dispersed. The distorted hot-streak showed the most complex transport behaviour through the stage. Results also revealed that the leakage flow through the rotor tip gap generated high heat transfer rates, in particular on the rotor blade suction side and tip surface. The leakage flow formed the known leakage vortex at the tip gap exit, which induced high heat transfer rates. The residual swirl was found to intensify the leakage vortex and consequently higher heat transfer rates are generated compared to the uniform flow condition.



## 1. Introduction

The new generation of aero-engines operate under a lean-burn combustion regime in order to reduce emissions threatening the environment (i.e. $CO_2$ and NOx). Lean-burn combustors generate highly swirled flows to attenuate combustion peak temperatures by enhancing the fuel-air mixing. The hot swirling flow attenuates as it propagates through the combustor and interacts with the coolant air from the combustor liner. However, a residual swirl persists at the turbine inlet and it features non-uniform aerothermal characteristics. These non-uniformities composed of the residual swirl and hot-streak that impact the turbine aerothermal performance [1–5].

The isolated effects of the residual swirl only, or the hot-streak only on the aerothermal performance of high-pressure turbines (HPT), are well studied in the literature, on either non-rotating vanes or rotating turbine stages [6–17]. Key experimental and computational fluid dynamics (CFD) findings from such isolated effects studies are summarised below.

### 1.1. Effects of the residual swirl

In an early study, Shih and Lin [6] reported a computational investigation on a turbine vane that features a leading edge (LE) fillet with a modified shape under both inlet axial flow and residual swirl conditions. They mentioned that the modified LE fillet under inlet swirl can deliver both lower aerodynamic loss and heat transfer rate. The total pressure at the vane exit plan was reduced by more than 40%, with respect to the axial flow case. Heat transfer coefficient was also decreased by more than 30% on the end-

* Corresponding author.
*E-mail address:* zakaria.mansouri@nottingham.ac.uk (Z. Mansouri).

https://doi.org/10.1016/j.ijheatmasstransfer.2022.123143
0017-9310/

walls and by more than 10% on the vane surface, with respect to the axial flow case. Over the past decade, the research turbine so called MT1 has been extensively investigated under aggressive swirl conditions in the Oxford Turbine Research Facility (OTRF) [7–9]. Qureshi et al. [9] carried out a combined detailed experimental and CFD investigations of the impact of aggressive residual swirl on both the aerodynamic and thermal characteristics of the stator vane of the MT1 turbine. A combustor swirl simulator was designed for this purpose [7]. It was found that the residual swirl remarkably altered the endwall flow structures and vane aerodynamic load. The boundary layer exhibited streamline redistributions, where they were dissipated in certain regions and converged in other regions. Under these redistributions, local Nusselt number significantly changed. Moreover, Schmid and Schiffer [10] simulated the impact of the residual swirl generated from an upstream combustion chamber on the aerodynamic characteristics (i.e., losses and secondary flows) and heat transfer of a downstream linear cascade vane. The modelled combustion chamber did not comprise of swirlers but the effect of the swirling flow was generated by imposing a tangential velocity boundary condition at the inlet. The authors investigated three main parameters, which are: the intensity of the swirl, the clocking position of the swirl centre and the rotation orientation (positive or negative). They noted that the increase in swirl intensity led to an increase of pressure loss downstream the vane and a decrease in the heat transfer rate within the vane passage. The heat transfer coefficient reached its maximum values on both the vane surface and endwalls when the swirl was negative and its core is in front of the vane LE.

### 1.2. Effects of the Hot-streak

Povey et al. [11] experimentally measured the heat transfer variation at the midspan (50%) of a HPT uncooled vane as well as on endwalls under hot-streak and uniform temperature. The clocking position of the hot-streak was also investigated. They reported that the vane facing a hot-streak has higher heat transfer rate on its suction side (SS) compared to the vane facing a uniform inlet temperature. A hot-streak positioned on front of the vane LE generates more heat transfer rate than a hot-streak positioned on front of the passage. Smith et al. [12] studied numerically the effects of hot-streak clocking position on a HPT stage. They reported that the aligned hot-streak with the vane LE produces higher thermal load on the vanes and lower thermal load on the rotor blades. In this case, the impingement of the hot-streak onto the vane LE spreads out due to the endwall vortices and radial pressure gradient, which results in lowering the temperature variations at the rotor inlet. For the case of the hot-streak aligned with the passage, it was not disturbed when convected through the vane and generated relatively high enthalpy levels on the pressure side (PS) of the rotor blades. Salvadori et al. [13] investigated the aerothermal performance of the MT1 turbine under hot-streak and uniform temperature using experimental measurements and numerical simulations. They found that for the vane, the hot-streak increased the heat transfer rate by 20% on the PS and 50% on the SS with respect to the uniform case. For the rotor blades, it was shown that the hot streak transport has affected the PS between 20% and 70% of the span, where the Nusselt number exhibited an increase of 60% with respect to the uniform case. Wang et al. [14] conducted an unsteady computational investigation on the so called GE-E3 turbine under the effect of hot-streak at different turbulence intensities. They reported that the increase of turbulence intensity from 5% to 20% led to a favourable temperature gradient on the rotor surface. At the LE, the temperature decreased by 16 K and at the PS, it was decreased only by 7 K. However, endwall temperature increased by more than 20 K, which represents 2.8% of the averaged inlet temperature. Very recently Mansouri [15] performed an unsteady computational investigation on a HPT stage to examine the interaction between three different hot-streak maps and secondary structures from the rotor blades. Two simplified hot-streaks (radial and circular) from the literature and one distorted hot-streak at aero-engine representative conditions were evaluated. It was revealed that the rotor blade generated many complex secondary flow structures and the boundary layer on its surface underwent turbulent/laminar transitions. The hot-streak migration and its impingement onto the vane and rotor blades differed from one hot-streak map to another. The secondary flows had a non-negligible effect on the stage exit temperature distribution. They generated corrugated and wavy shapes on the temperature gradients, in particular near the hub and shroud. All hot-streaks were completely dispersed and deformed across the turbine rotor. Hot temperatures are found on the rotor surfaces for the radial and distorted hot-streaks compared to the relatively mild temperature from the circular hot-streak.

During the last few years, the effects of the residual swirl and hot-streak simultaneously on HPT vane aerothermodynamics has gained a particular attention. Many studies are now available in the literature [18–24]. However, works on combined residual swirl and hot-streak effects on rotating HPTs are rare in the literature [25–30]. The majority of these works are numerical and they adopt an idealized circular or elliptical hot-streak shapes, which are not representing realistic distorted shapes generated by aero-engine combustors. Main findings from such combined effects studies are summarized below.

### 1.3. Combined residual swirl and hot-streak effects on vanes

Griffini et al. [19] performed a CFD investigation on the impact of combustor exit flow representative of aero-engine conditions on a film cooled HPT vane. The combustor flow characteristics were obtained from a previous European project called TATEF2 [20]. The clocking positions of the residual swirl were also investigated. They found that the case where the residual swirl is aligned with the vane LE had the harshest characteristics. This case presented high heat transfer rates accompanied with increased local and averaged surface temperature on both the vane SS and PS compared to the passage aligned swirl. More recent work was reported by Andreini et al. [21] and conducted within the European project called FACTOR that was interested in the effects of combined swirl and realistic hot-streak on HPTs aerothermal behaviour. The authors designed a non-reacting annular combustor equipped with effusion cooling liners and axial swirlers with and without connecting tubes to generate aero-engine representative conditions. The combustor was investigated both experimentally and numerically. Results of this work showed that the annular combustor generates high swirling flow intensity and distorted hot-streak, which differ from the widely used rounded hot-streaks in the literature. In addition, their generated distorted hot-streak maps with and without connecting ducts were quasi similar. Wang et al. [22] conducted conjugate heat transfer simulations on a film-cooled vane to reveal the impact of the residual swirl and hot-streak on the film cooling performance. They investigated two setups with hot-streak only and four setups of combined swirl and hot-streak involving two swirl orientations and two clocking positions. The results indicated that the presence of residual swirl worsen the attachment of the coolant film and increased the thermal load on vane surfaces. Among the four swirled setups, the one with negative swirl orientation aligned to the vane LE was found to be the best choice as it has reduced the temperature on the vane LE and PS compared with the other setups. The more recent numerical study by Mansouri [23] on the impact of three different distorted hot-streaks at engine representative conditions on a HPT vane was carried out

under axial and swirl flow conditions. The results showed significant differences in the aerothermal field on the vane cascade under each distorted hot-streak. The presence of swirl induced aerothermal mixing and resulted in an increase of the heat transfer rate on all cascade surfaces (i.e., SS, PS, hub and, shroud).

### 1.4. Combined residual swirl and hot-streak effects on turbines

Khanal et al. [27] reported a CFD study on the MT1 turbine to examine its aerothermal behaviour under combined swirl and hot-streak. They found a distinctive radial transport of the hot-streak across the vane and rotor passages with strong impact on the turbine performance. They also highlighted that the rotor blade heat transfer behaviour is strongly dependent on the clocking position and swirl direction. Rahim and He [28] performed a computational investigation on a HPT stage with leaned vanes exposed to a simultaneous residual swirl and hot-streak. They reported similar finding to those in the literature [22,23,26] regarding the radial migration of the hot-streak through the vane under the effects of the swirl. They also concluded that the rotor inlet total temperature profile and rotor blade heat transfer rate were significantly altered under the effects of the swirl. Wang et al. [30] conducted a sophisticated CFD analysis of the effects of combined residual swirl and hot-streak on both film-cooled vanes and rotor blades of the GE-E3 turbine. They revealed that under uniform inlet conditions (no swirl and no hot-streak) the film cooling effectiveness fluctuations at the rotor LE are the most important with an amplitude of ±100%. Under combined swirl and hot-streak conditions, the coolant attachment and film cooling effectiveness were altered. The time-averaged film cooling effectiveness on the rotor blade SS and PS was reduced by 10% and 6%, respectively with respect to the uniform case. Very recently Adams et al. [31] conducted the first joined experimental and CFD investigation on the impact of combined realistic hot-streak and swirl on a 1.5 stage film-cooled turbine. They conducted the experimental measurements on the new research turbine called LEMCOTEC in the OTRF, which has been designed to represent new generation aero-engine operating conditions and architectures. They considered two HPT inlet flows with uniform and non-uniform characteristics (i.e., total temperature, flow angle and total pressure). Both measurements and computations suggested that the hot-streak was relatively well preserved after crossing the turbine stage. Total temperature fluctuation at the turbine exit was approximately double for the non-uniform case by comparing with the uniform case. The combined swirl and hot-streak induced changes in the rotor aerodynamics by causing local attenuations in blade loading near the hub and a reduction in tip leakage flow losses were decreased.

With the very remarkable advances in the present subject made through the investigations mentioned above and many others available in the literature, all investigated hot-streak shapes in rotating HPT stages were ideal, either circular [25–29] or elliptical [30]. To date, there is only the very recent study by Adams et al. [31] that investigated the impact of representative aero-engine combustor exit conditions on a rotating HPT. Thus, the present investigation is mainly motivated by the need to further understand and examine the effects of aero-engine combustor exit conditions on the rotating blades of HPTs. These effects cannot superimpose linearly when studied individually and their understanding is crucial for turbine aerothermal and cooling designs. This investigation presents the first computational study that compares and highlights the difference between the effects of lean burn combustor hot-streak and ideal hot-streaks from the literature under swirl conditions on the aerothermodynamics of a rotating HPT. To this purpose, numerical simulations using unsteady Reynolds-averaged Navier–Stokes (URANS) have been carried out on three hot-streak topologies (radial, rounded and distorted) under axial and swirl inlet flow conditions. Results of the different cases are compared and discussed. The position of each investigated hot-streak is fixed in front of the vane LE, and the clocking effect is not treated in the present work. In our recent work on the present turbine configuration [15], it was shown that that the hot-streak aligned with the vane LE produces higher thermal load on the vane and lower thermal load on the rotor blades. When the hot-streak is aligned with the vane passage it generates higher thermal load on the rotors.

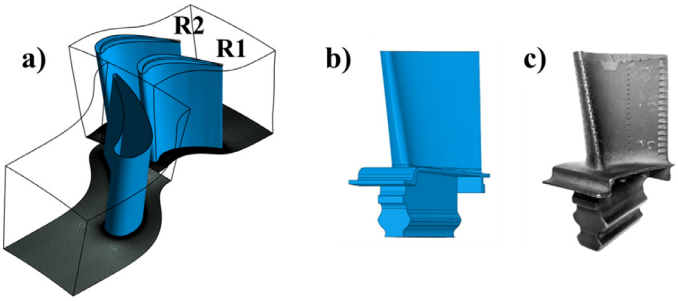


**Fig. 1.** Single passage domain of the HPT (a), the modelled uncooled rotor blade (b) and the real cooled rotor blade (c).

## 2. Turbine stage configuration

The configuration investigated in the present study is a first stage turbine uncooled model representative of a turbofan HPT composed of 36 vanes and 70 rotor blades. Since the rotors-to-vanes count ratio is almost equal to 2, a single passage geometry composed of one vane and two rotor blades can easily be adopted with periodicity boundary conditions as shown in Fig. 1(a). Thus, changes in blades count (e.g., using domain scaling method [29]) to enable single passage domain periodicity is not required for the present configuration. Adopting a single passage is an effective way to reduce the computational cost associated with full annulus modelling, but this is not without issues. When a turbomachine experiences a rotating instability that propagates between the neighbouring blades, standard periodic boundaries cannot resolve this phenomenon. The vane/rotor interface of the present passage is located at the mid distance between the vane TE and the rotor LE. The turbine vane is an uncooled annular cascade developed and investigated by NASA [32]. It was designed for a fully axial flow incidence angle. It has a chord length of 0.055 m, a height of 0.038 m and an exit flow angle of 67°. The modelled rotor blade is shown in Fig. 1(b) and it is derived from a real turbofan HPT rotor shown in Fig. 1(c). It features the following characteristics on its mid-span: an axial chord length of 0.029 mm, a solidity of 0.75, and a turning angle of about 120°. The rotor tip-gap height is a fraction of 1% from the passage height. The blade model has not been experimentally investigated before. It features a variable spanwise thickness, it is twisted, uncooled, highly cambered and without squealer tip. Fig. 2

## 3. Numerical setup

The numerical grid used for the present investigated turbine stage is a multi-block type, fully structured and was created using ANSYS-TurboGrid. The vane passage has 1.12 million points and a single rotor blade 1.77 million points, which leads to a total 4.68 million point for the simulated HPT stage passage. The thickness of the cell adjacent to the turbine stage walls (hub, shroud, vane, and rotor blade) is fixed at values that guarantee the $y^+$ around 1. This $y^+$ value is required by the employed turbulence model k-$\omega$ SST $\gamma$-$Re_\theta$ [37] to properly predict the flow transition and/or boundary layer separation. The tip gap is discretised with 44 cells to pre-

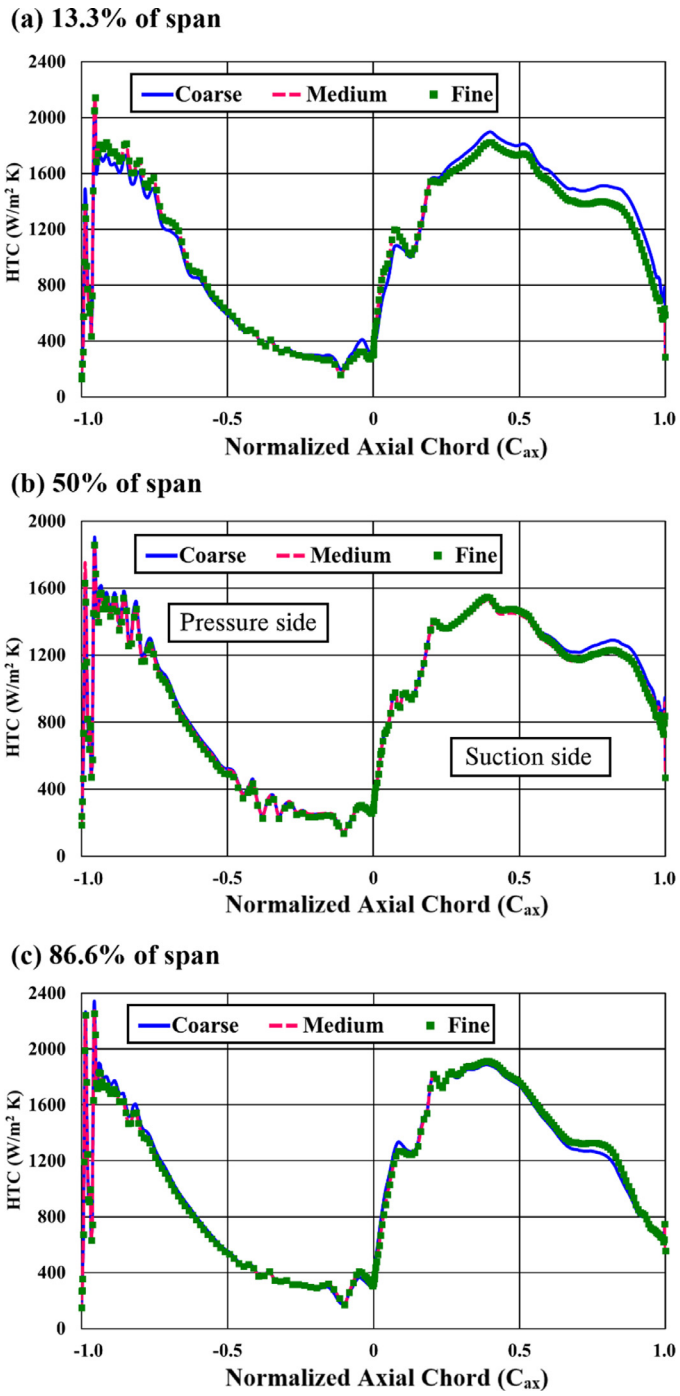


**Fig. 2.** Heat transfer coefficient profiles for the three investigated meshes on the vane surface at different span locations (a) near the hub, (b) at the midspan, and (c) near the shroud.

dict correctly the velocity and temperature profiles of the leakage flow. This value is selected based on the work of Rahman et al. [39]. The number of grid points of the vane and rotor blade domains was carefully selected after a grid sensitivity analysis, which can be found in our previous works [15,18,23,33,34]. An example of the heat transfer coefficient (HTC) distribution at different span locations on the vane surface using three different meshes is given in Fig. 3. The meshes are coarse, medium and fine, and they contain 0.6, 1.2 and 2.7 million cells, respectively. It can be seen that the medium and fine meshes have the same HTC profiles at the different span locations, whereas the coarse mesh has some discrepancy at the suction side region of the vane, which is large near to the hub location (e.g., $C_{ax}$ = 13.3 %). Thus, the medium mesh density is used within the vane domain of the turbine stage.

Detailed validation with experimental measurements [32,35] has been also conducted for both the vane and rotor blade. For the vane, a fully axial flow with uniform total pressure is imposed at the inlet and a static pressure is specified at the domain exit. The exit-static to inlet-total pressure ratio is 0.6705. The inlet and outlet are located at one axial chord length from the vane leading edge and trailing edge, respectively. Two periodic boundaries are imposed at the side surfaces of the vane domain and all the walls are considered adiabatic with non-slip condition. Figs. 3(a-c) show comparisons of the experimental [32] and computed surface-static to inlet-total pressure ratio distributions at different span locations on the vane surface. It can be seen that the predicted pressure ratio profiles are in good agreement with the experimental measurements at the midspan and endwall regions. The results near the endwall (e.g., $C_{ax}$ = 13.3% and 86.6%) confirm that the employed grid and turbulence model are able to capture the effects of secondary flows on the blade load. Fig. 3.d shows comparison of the experimental [32] and computed circumferentially averaged loss coefficient downstream the vane. The numerical loss profile is in good agreement with the experimental profile and confirms that the employed modelling can properly predict the penetration of the secondary flows in the main flow.

For the present rotor model used, there are no experimental measurements available in the literature. Thus, an experimental rotor blade called R1S1 [35] that features the same turning angle and thickness-to-chord ratio at the midspan has been adopted for the validation. Note that the experimental results of the R1S1 blade are only reported at the midspan and no measurements near the endwall or tip regions are conducted. The validation condition used corresponds to an isentropic Mach number of 0.75, where a uniform total pressure is imposed at the rotor domain inlet with a constant turbulence intensity of 4% and a length scale equal to the blade span. At the outlet, a static pressure is specified. All the walls are adiabatic with non-slip condition. Fig. 4 shows distributions of the numerical HTC compared to experimental measurements. The computational results from both the original SST model [36] and the transition SST $\gamma$-$Re_\theta$ model [37] are compared. It can be seen that the blade SS faces boundary layer transition between the upstream and the mid chord (e.g., $C_{ax}$ = 0.5) regions. The original SST model fails to capture this transition. The transition SST $\gamma$-$Re_\theta$ model underestimates slightly the length of the transition, but it provides good agreement with the experimental measurements at the rest of the locations. The slight discrepancy of the transition length is due to the use of the default coefficients of the SST $\gamma$-$Re_\theta$ model, which are initially defined for simplified configurations and low Mach number flows. Enhancement of the validation can be achieved by the calibration of this model for each specific flow problem [40,41] (e.g., a transonic flow), but this is out of the scope of the present work.

Unsteady time accurate computations of the HPT stage were conducted using the CFX CFD solver. It is a three-dimensional implicit coupled Navier–Stokes solver, which uses the finite volume method for the spatial discretization. The high resolution option was selected for the spatial discretization, which is a second order central difference scheme. The second order backward Euler scheme was used for the time discretization. The solved equations are the mass conservation, Navier–Stokes flow momentum ($u$, $v$, $w$), turbulent kinetic energy ($k$), specific dissipation rate and energy ($\omega$). The turbulence was handled using the Shear Stress Transport (SST) k-$\omega$ model [36] with transition formulation based on the Gamma-Theta ($\gamma$- $Re_\theta$) approach [37], as previously performed in the validation with experimental measurements. This model solves the momentum and turbulence transport equations

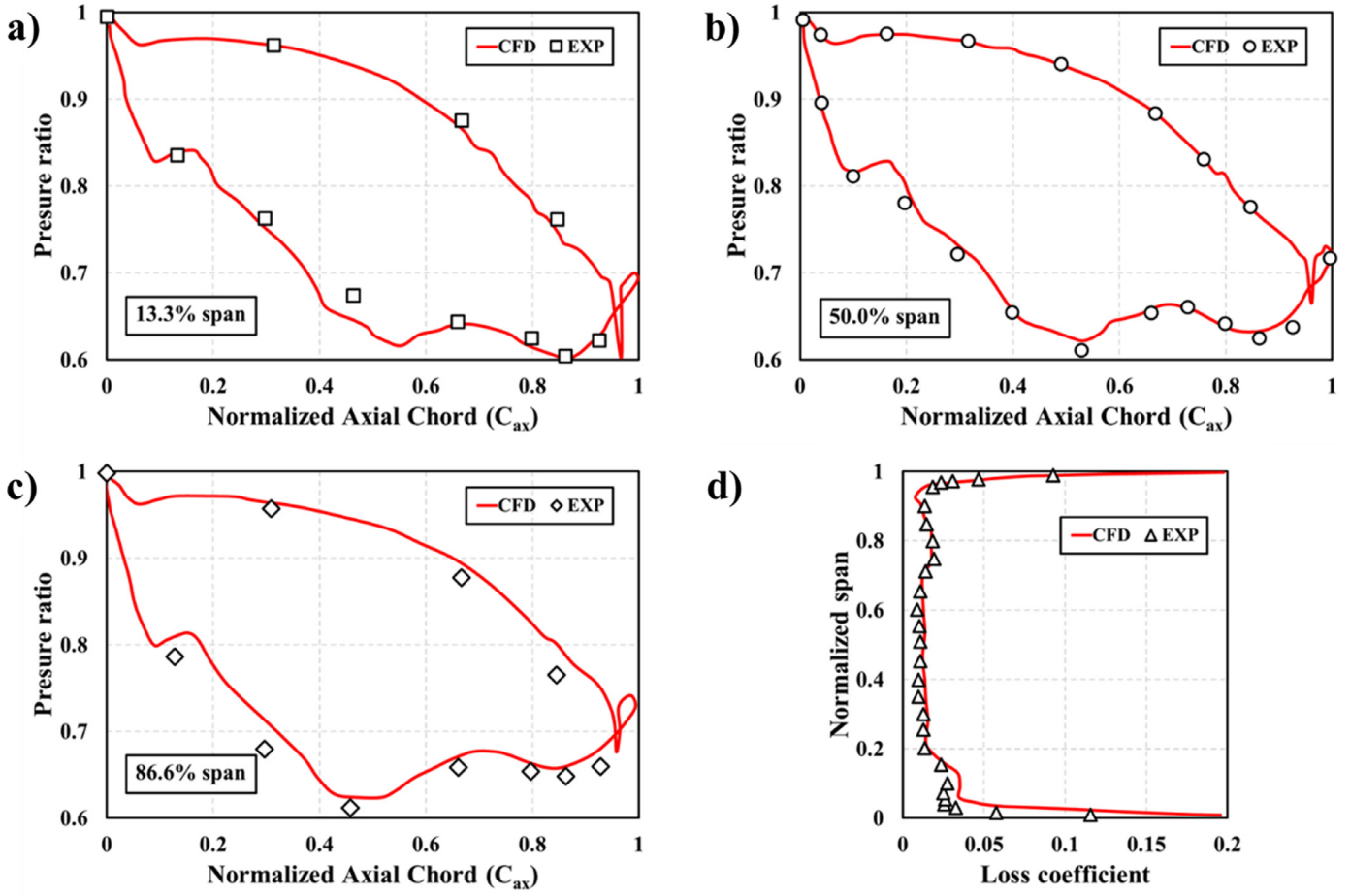


**Fig. 3.** Comparison between the measured and predicted pressure ratio on the vane surface at (a) the near hub, (b) the midspan and (c) the near shroud, and (d) loss coefficient downstream the vane.

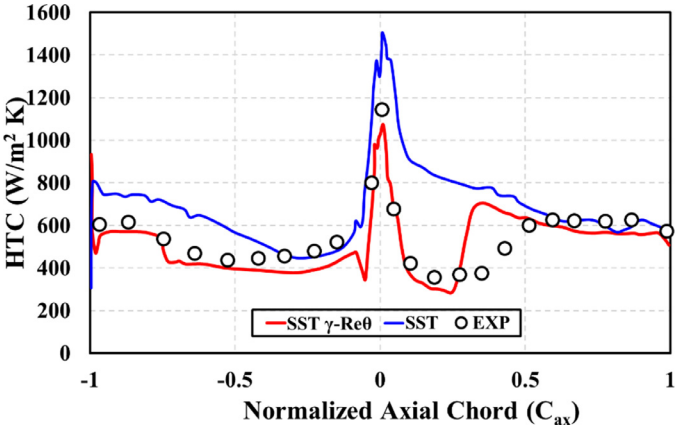


**Fig. 4.** Comparison between measured and predicted heat transfer coefficient of the rotor blade surface at the midspan.

mentioned above as well as three additional transport equations for the shear stress ($\tau$), the intermittency ($\gamma$), and the transition Reynolds number ($Re_\theta$) near the wall (withing the boundary layer). Thus, the boundary layer flow is resolved, and no wall function is used. A transient rotor-stator method was used at the interface between the stationary vane and rotor domains. Only one full rotor rotation is modelled with time periods equal to the rotor blade pitch (5.14°), each period is simulated with 25 time steps, which leads to a time step $\Delta t = 4.89 \times 10^{-6}$ second, and each time step is achieved with a minimum 25 sub-iterations. This time step is selected based on the work of Rahman et al. [34] where they conducted a sensitivity analysis on the time discretisation using 20, 40, and 60 time steps for a time period equivalent to 12° stator vane pitch for a high pressure turbine rotating under 9500 rpm. They found that a vane passing period discretised with 40 time steps leading to a $\Delta t = 5.26 \times 10^{-6}$ second is sufficient to reach a temporal convergence. Thus, the present used time step is quite below the optimal value found by Rahman et al. [39].

The adopted boundary conditions were imposed as follows. Two-dimensional static temperature contours representing the hot-streaks were specified at the stage inlet with a uniform total pressure distribution based on the constant pressure combustion assumption in gas turbines. Note that Adams et al. [31] used a realistic quasi-uniform total pressure distribution that has almost a negligible variation of around ±0.47%. In addition, a constant turbulence intensity $I = 10\%$ is imposed at the inlet, which may not be representative to real aero-engine conditions, but this assumption is adopted in many available studies [28–31]. The inlet length scale is auto-computed by the solver based on the specified turbulence intensity, as follows [38]:

$$l_t = \frac{k^{3/2}}{\varepsilon_{in}} = \frac{(3/2)I^2U^2}{\rho C_\mu \left(k^2/1000\mu\right)} \quad (1)$$

where $l_t$ is the length sacale, $k$ is the turbulent kinetic nergy, $\varepsilon$ is the turbulence dissipation, $U$ is the average flow velocity, $\rho$ is the fluid density, $C_\mu$ is a model constant equal to 0.09, and $\mu$ is the fluid dynamic viscosity.

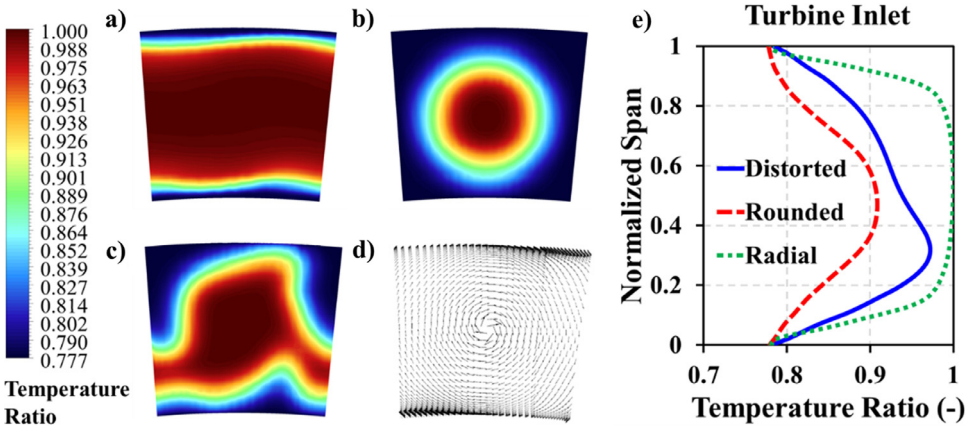


**Fig. 5.** Static temperature maps of the hot-streaks (a) radial, (b) rounded, and (c) distorted. (d) velocity vectors showing residual swirl and (e) circumferentially averaged hot-streak radial profiles.

An atmospheric static pressure was specified at the stage outlet. The exit isentropic Mach number is transonic around 1. The HPT stage operates with the air as an ideal gas. The rotor blades domain rotates at a speed of 7000 rpm. All walls are assumed adiabatic with a non-slip boundary condition. To investigate the effects of hot-streak transport through the turbine, three different static temperature topologies are applied at the turbine inlet, as shown in Fig. 5. Radial and rounded idealized topologies from the literature are adopted and shown in Figs. 5(a) and 5(b), respectively. The radial hot-streak includes the effect of film cooling from a combustor liner near the endwalls and a constant high temperature of about 80% of the map. The rounded hot-streak features a high temperature level focused circularly on the centre of the map representing an ideal thermal gradient from a swirled combustor. Such ideal temperature gradient has been a subject of many investigations in the literature [11–14,26–30]. A distorted hot-streak topology is also considered and shown in Figs. 5(c). It was generated by a lean-burn combustor simulator designed and scaled to fit the present HP turbine stage [23]. The combustor can operate using swirl injectors of different sizes, angles and arrangements that can generate different distorted temperature topologies representative of modern aero-engine combustor outflows [23]. The distorted hot-streak features a large deformed hot temperature core aligned with the vane LE and connected to a bottom hot strip. It is interesting to note that the applied hot-streaks have different pitchwise and spanwise extensions (e.g., the distorted hot-streak is much larger than the rounded one), so that the thermal results are expected to be influenced not only by the hot-streak shapes but also by their sizes. Note that all the investigated topologies have a minimum-to- maximum temperature ratio $T_{min}/T_{max}$ of 0.78. Circumferentially averaged radial profiles of the temperature ratio of each hot-streak are plotted in Fig. 5(e). The residual swirl distribution used along with the hot-streaks is shown in Fig. 5(d). It is aligned with the vane leading edge and rotates in the clockwise direction. The swirl intensity used is $S_i = 0.4$ and its defined based on the swirl injector geometry in the combustion chamber and flow velocity [42,43].

$$S_i = \frac{\int_{R_i}^{R_o} UWr^2 \mathrm{d}r}{\int_{R_i}^{R_o} R_n U^2 r \mathrm{d}r} \tag{2}$$

with $r$ is the radius of the swirler $R_i$ and $R_o$ are the inner and outer radii of the swirler, respectively. $W$ is the average swirling velocity and $U$ is the average axial velocity. Moreover, the swirl intensity equation could be reduced to include only the axial and swirling velocities, such as $S_i = W/U = 0.4$ [43].

Unsteady simulations were initialized from converged steady solutions based on the frozen rotor approach to model the vane/rotors interface. The root-mean-square (RMS) residuals of all solved equations were below $10^{-5}$. During simulations, difference physical quantities at different locations were monitored to ensure the periodic behaviour of the unsteady flow. These quantities are the static pressure, the static temperature, the mass flow rate and the total pressure. The monitoring locations are the blades surface (vane and rotor), the interface and the stage exit. A typical unsteady convergence of the area-averaged total pressure difference at the interface and normalized exit mass flow rate for the distorted case are given in Fig. 6. A transition from the steady to the unsteady solution occurs quickly after few timesteps, and the periodic oscillation of the solution remains constant till the last timestep. It is interesting to note that the area-averaged total pressure difference between the stationary vane exit and the rotating blade inlet non-conformal faces does not exceed 30 Pa (Fig. 6(a)), which represents a fraction of 0.029% of the atmospheric pressure, for example. This result confirms that the adopted transient rotor-stator method is very robust and produces a negligible error. A Fast Fourier Transform (FFT) analysis for the total pressure difference recorded signal at the interface was performed and shown in Fig. 6(c). Two harmonics are predicted showing the blade passing frequency (BPF = 8171 Hz) where the second harmonic represents 23% of the energy contained in the BPF. Note that the number of harmonics is sensitive to the probe location [45] (e.g., near the midspan or the endwalls), the probed quantity [46] (e.g., static pressure, axial velocity, turbulent kinetic energy, etc.). However, the adopted URANS model (SST $\gamma$-$Re_\theta$) showed that it is capable to predict the same number of harmonics compared to Large Eddy Simulation (LES) as reported in [47].

## 4. Results and discussions

It is important to note that the results presented in this section are related to the rotor domain, which is the main focus of the present study. Results of the effects of combined distorted hot-streak and residual swirl on the vane are already published in [23].

### 4.1. Hot-streak transport

Fig. 7(a) shows the radial profiles of static temperature ratio at the rotor inlet (vane outlet), with uniform (no swirl) and swirl inlet conditions for each hot-streak case. With uniform flow conditions, all profiles keep their initial radial distributions (from the turbine inlet) with maximum values at around 30% span, 50% span and 30-70% span for the “Distorted”, “Rounded” and “Radial” cases,

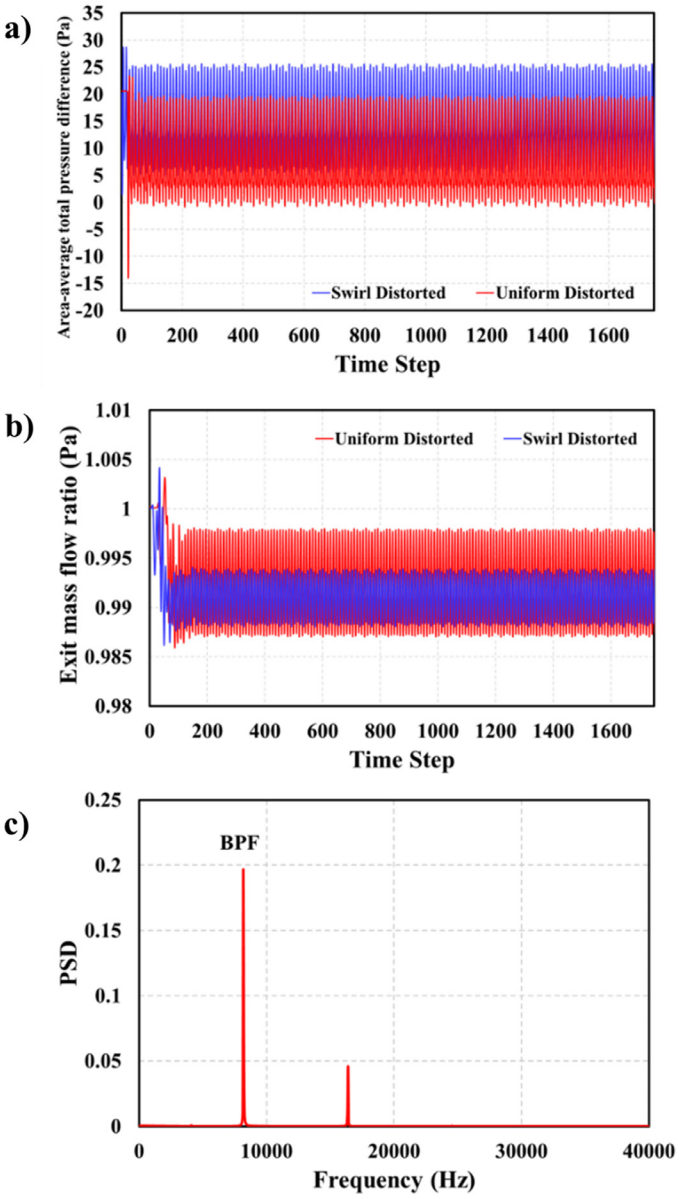


**Fig. 6.** Periodic convergence (a) area-average total pressure difference at the interface, (b) normalized mass flow rate at the outlet, and (c) FFT of the total pressure difference.

respectively. However, a slight reduction in temperature between turbine inlet and rotor inlet is found as expected and this is due to the compressibility effects as the flow crosses the vane passage as the Mach number increases and the static temperature decreases. With inlet swirl condition, temperature profiles of all the hot-streak cases exhibit almost the same flattened distribution. The averaged value of each of the flattened profiles varies significantly, which are 0.83, 0.79, and 0.9 for the distorted, rounded, and radial hot-streaks respectively. These values reflect the sizes of the imposed hot-streaks as previously mentioned. The introduction of swirl enhances the aerothermal mixing and reduces the levels of temperature peaks. Fig. 7(b) presents the same profiles at the rotor outlet. The profiles of the uniform flow condition are redistributed again after traveling through the rotor passages. This redistribution is mainly caused by the interaction with secondary flows (i.e. tip leakage and passage vortices). With inlet swirl condition, temperature profiles of all hot-streak cases kept almost flattened distributions, since the effects of swirl mixing persist within the rotor passage and may be also intensified by the secondary flows.

The transport of hot-streaks through the rotor passage is visualised using instantaneous static temperature ratio contours at four plans located at the normalized spanwise direction (Z) as indicated in Fig. 8. The first location Z=1.0 is at the vane/rotor interface, the second location Z=1.1 is across the rotor blades LE, the third location Z=1.35 is across the rotor blades TE, and the last location Z=2.0 is at the stage outlet.

For the "Radial" hot-streak case (Fig. 8(a)) and under uniform inlet flow, it can be seen that the hot-streak shape at the rotor inlet (Z=1.0) and LE (Z=1.1) is almost preserved. The wake from the vane has a very slight effect on it and the cold regions representing the film cooling from the combustor are still located the endwalls. After crossing the rotor blades and on the rotor blade TE (Z=1.35), the upper and lower cooling films exhibit a roll-up and are driven inside the passage due to the interaction with the secondary flows. The rolling-up near the shroud seems more intense compared to the rolling-up near the hub and this indicates that the leakage vortex (LV) formed near the tip is stronger than the passage vortex (PV) formed near the hub. At the exit (Z=2.0), the gradient from the cold to the hot regions is no longer smooth and it presents a corrugated wavy shape as highlighted by the red dashed line. In addition, the maximum temperature ratio is decreased from 0.961 at the rotor inlet to 0.856 at the exit due to the compressibility effect and the increase of the flow velocity. For the same hot-streak (radial), as the swirl motion is introduced, the temperature maps at all spanwise locations exhibit a deformation. The swirl applies a strong mixing on the flow field and consequently the near endwall cold regions are transported radially towards the mid-passage to be mixed with the hot region (i.e. see the black dashed line at Z=1.0). For example, the mid-passage region between the rotors (R1 and R2) at the TE (Z=1.35) features a relatively cold temperature compared to the same location under no swirl. Moreover, the LVs are filled with high temperature for both uniform and swirl conditions at Z=1.35 and this suggests that the leakage flow, originated from the blade PS, drives the hot fluid from this region through the tip gap to the LV core. At the exit, the

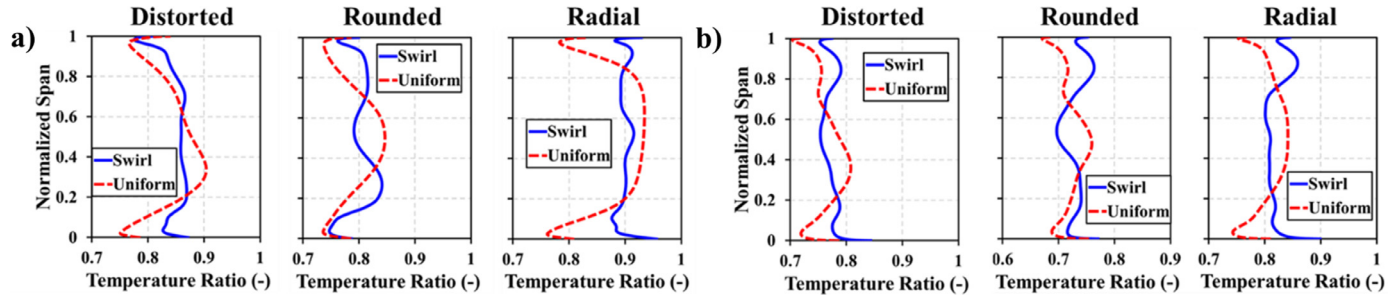


**Fig. 7.** Radial profiles of the circumferentially averaged static temperature for the different investigated hot-streaks under uniform and swirl conditions: (a) profiles at rotor inlet and (b) profiles at rotor exit.

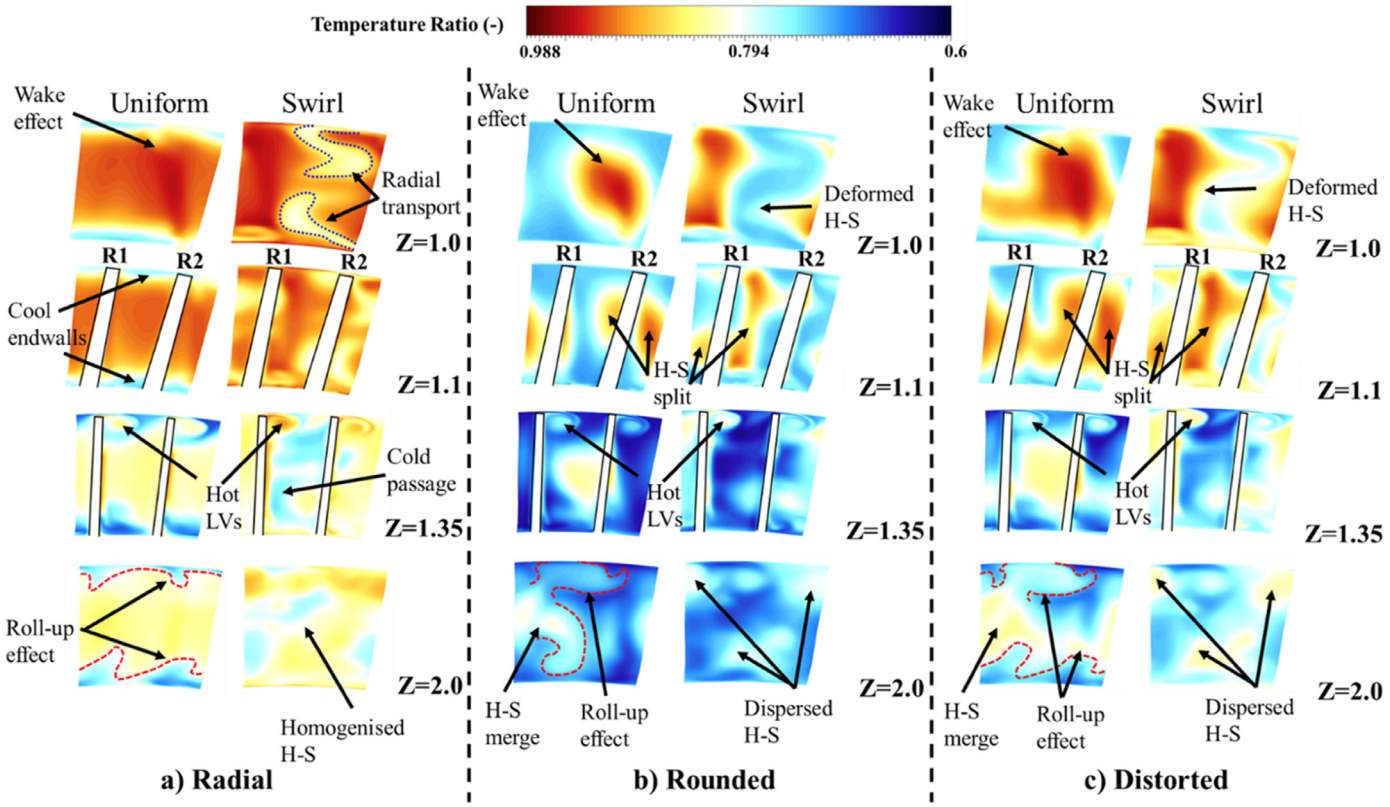


**Fig. 8.** Transport of the hot-streak under uniform and swirl conditions at different locations through the rotor passage using instantaneous static temperature contours (a) radial, (b) rounded, and (c) distorted cases.

radial hot-streak is homogenised mainly under the swirl effect and the cooling film is spread to form some cold spots.

For the "Rounded" hot-streak (Fig. 8(b)) under no swirl, it is transported axially as expected and the highest temperature levels are preserved within the mid-span region. The vane wake has a remarkable impact of the hot-streak at the rotor inlet (Z=1.0) where the round shape becomes elliptical. The hot-streak travels to impinge onto the rotor R2 LE and is split into two parts (Z=1.1). Then, a portion from each part of the split hot-streak travels from the PS to the SS through the rotor tip to form the hot LVs (Z=1.35). At the exit (Z=2.0), each part of the split hot-streak merge to form a single hot-streak that is completely deformed with a hot region always around the mid-span region. As the swirl is combined with the "Rounded" hot-streak, this later exhibits a deformed shape at the vane exit (Z=1.0). The rounded shape becomes elongated from the hub to the shroud with a wavy low temperature gradient separating each hot-streak. The new deformed hot-streak travels mainly between the rotors and only a small part of it impinges onto the rotor R1 LE near the hub (Z=1.1). The LVs formed around the blade TEs are always hot (Z=1.35) with temperature ratios of 0.801 and 0.775 for the LVs for the R1 and R2, respectively. At the exit (Z=2.0), the hot-streak becomes dispersed around all the plane with many hot spots at different locations.

The "Distorted" hot-streak (Fig. 8(c)) under uniform flow exhibits an axial convection through the rotor passage similar to the "Rounded" case. The vane wake has a slight effect on changing the hot-streak shape at Z=1.0. When traveling through the passage, the hot-streak impinges onto the rotors both (Z=1.1), the large hot core hits the second rotor R2 and the hot strip hits the first rotor R1. Both hot-streak parts contribute to the formation of hot LVs similar to the "Rounded" case (Z=1.35). At the stage outlet (Z=2.0), the split hot-streak merges again and it is highly affected by the roll-up effect from the secondary flows near the endwalls. The maximum temperature ratio at this location reaches 0.842, which is 12.38% lower than maximum temperature ratio at the turbine inlet. When the residual swirl is combined with the "Distorted" hot-streak, the temperature distribution through the rotor passage becomes more complex at each plan compared with the other idealised hot-streaks. The "Distorted" hot-streak becomes highly deformed and the original hot strip disappears (Z=1.0). It also becomes elongated from the hub to the shroud but with a complex behaviour compared to the elongated "Rounded" hot-streak at the same location. When interacting with the rotors it impinges onto the rotor R1 near the hub and onto the rotor R2 near the shroud (Z=1.1). It generates hotter LVs compared to the LVs of the "Rounded" case with the temperature ratios of 0.83 and 0.804 for R1 and R2, respectively. These values represent an increase of temperature of 3.49% and 3.6% with respect to the R1 and R2 LVs of the "Rounded" case. Finally, at the stage exit (Z=2.0), the hot-streak exhibits a highly dispersed behaviour with different large hot spots.

### 4.2. Rotor surface temperature

Fig. 9 shows instantaneous static temperature ratio distributions on the first rotor blade R1 surface at the tip and SS region. With uniform conditions (Fig. 9(a)), the temperature map from each hot-streak is transported axially as expected, where the highest temperature levels are located around the midspan region. The effects of the secondary flow vortices are clearly visible on the SS as the dashed line shows for the "Radial" case. The vortices cool down the near hub and tip regions on the SS since they radially transport the cool air from the endwall regions. The "Radial" case has the largest hot surface temperature zone, followed by the "Distorted" case and next the "Rounded" case. On the tip, the LE region has the lowest temperature compared to the mid chord region and this suggests

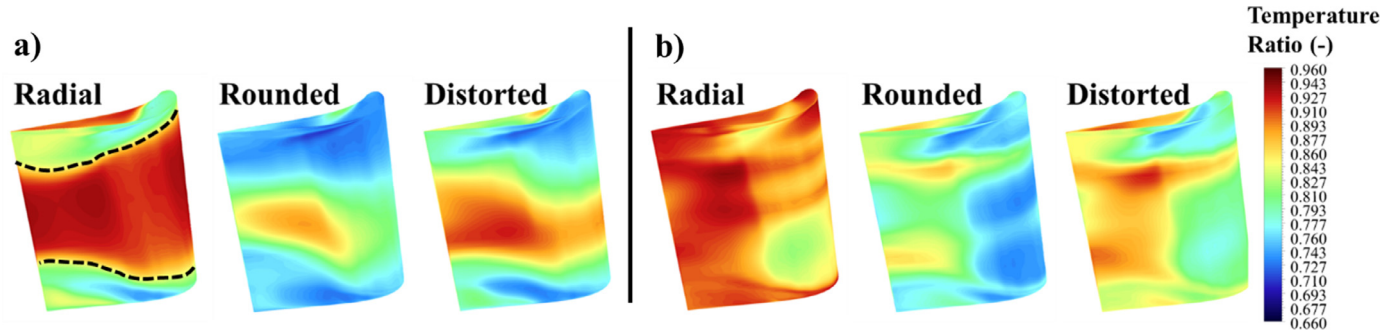


**Fig. 9.** Instantaneous static temperature on the rotor blade tip and SS for all the investigated hot-streaks: (a) with uniform inlet flow and (b) with inlet swirl condition.

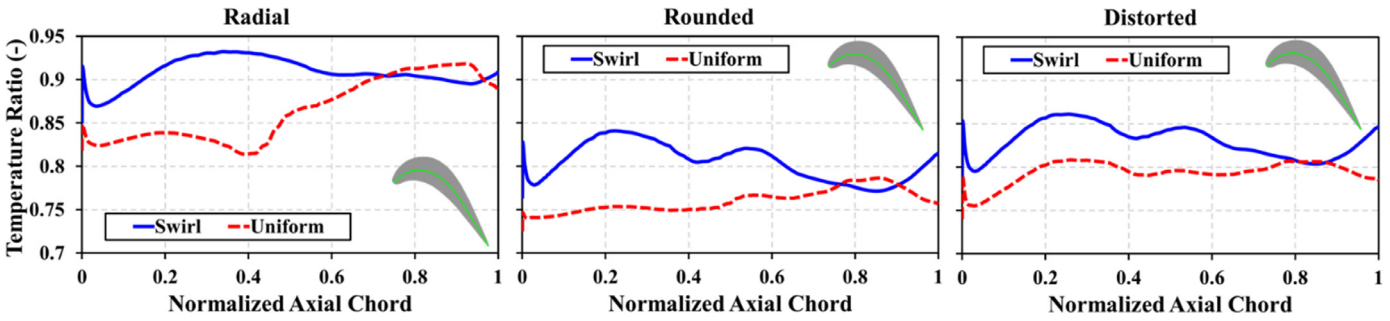


**Fig. 10.** Temperature profiles on the chord line of the rotor blade tip for all the investigated cases.

that the leakage flow transports the cold flow from the shroud towards the LE and the hot flow from the passage towards the mid chord region. As the inlet swirl is introduced (Fig. 9(b)), a complex change in the rotor thermal loading takes place. The effects of the secondary flows are attenuated and the temperature distribution on the blade surfaces does not reflect any more the initial temperature non-uniformity imposed on the turbine inlet. The "Radial" case under swirl has almost a uniform surface temperature distribution of low levels compared to the uniform case due to flow mixing, except a cold spot near the hub of the SS. In the "Rounded" and "Distorted" cases, the hot-streak is no longer printed on the midspan region but it is spread almost all over the span near the trailing edge region. On the tip surface, the mid chord region suffers from higher temperature levels compared to the uniform case due to the radial transport of the hot-streak. Generally, it can be said that the swirl has a significant impact on modifying the hot-streak distribution and simplified hot-streaks should not be used to represent engine operating conditions. The "Radial" case generates excess of high temperatures and the "Rounded" case a simpler predicted temperature distribution.

Fig. 10 shows static temperature ratio ($T_r$) profiles plotted through the chord line at the rotor blade R1 tip for all cases. One can note that the "Radial" case has the highest temperature under both uniform and swirling flow conditions. Under uniform condition, the temperature profile undergoes a jump at around Cax=0.4 from relatively low temperature ($T_r$=0.814) to high temperature ($T_r$=0.918) with an absolute maximum-to-minimum difference of 11.34% and an average value ($T_{r,ave}$) from the LE to the TE of $T_{r,ave}$=0.862. It was revealed above (Fig. 9(a)) that the jump to higher temperature is due to the transport of the hot flow by the leakage from the passage towards the mid chord region of the tip. Under swirl condition, the temperature profile presents high levels of temperature from the LE to the TE. This is due to the mixing effects from the swirl where the cooling film near the shroud is mixed with the large hot flow from the mid passage. Thus, the absolute maximum-to-minimum difference is decreased to 6.75% and the average value is increased to $T_{r,ave}$=0.907 with respect to

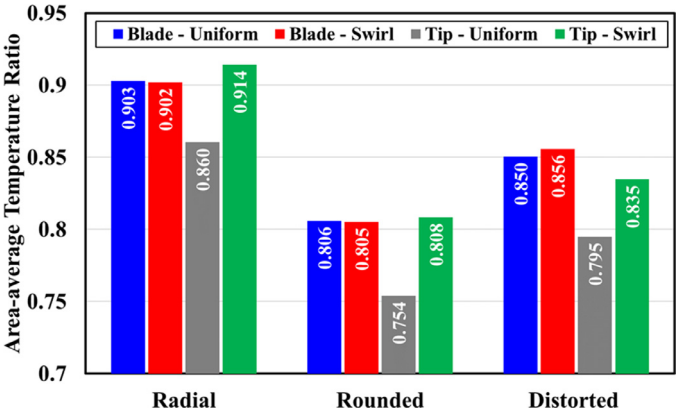


**Fig. 11.** Area-averaged static temperature of the rotor blade and tip surfaces for all the investigated cases.

the previous uniform case. For the "Rounded" and "Distorted" hot-streaks combined with the residual swirl, the temperature profiles undergoes an increase compared with the relatively low temperature profiles of the uniform condition. It became obvious that this increase was due to the mixing and it can be quantified by the following average values. For the "Rounded" case, the average temperature ratios are $T_{r,ave}$=0.756 and $T_{r,ave}$=0.807 for the uniform and swirl cases, respectively with an increase of 6.32%. For the "Distorted" case, the average temperature ratios are higher than those of the "Rounded" case and they take the value of $T_{r,ave}$=0.79 and $T_{r,ave}$=0.833 for the uniform and swirl cases, respectively with an increase of 5.16%.

The area-averaged temperatures on the blade and tip surfaces are of interest and are provided in Fig. 11 under both uniform and swirl conditions. The blade surface includes the SS and PS without the tip surface. It can be seen that the area-average temperature of the blade surface is almost unaltered under the residual swirl for the different hot-streaks. A very slight difference is ob-

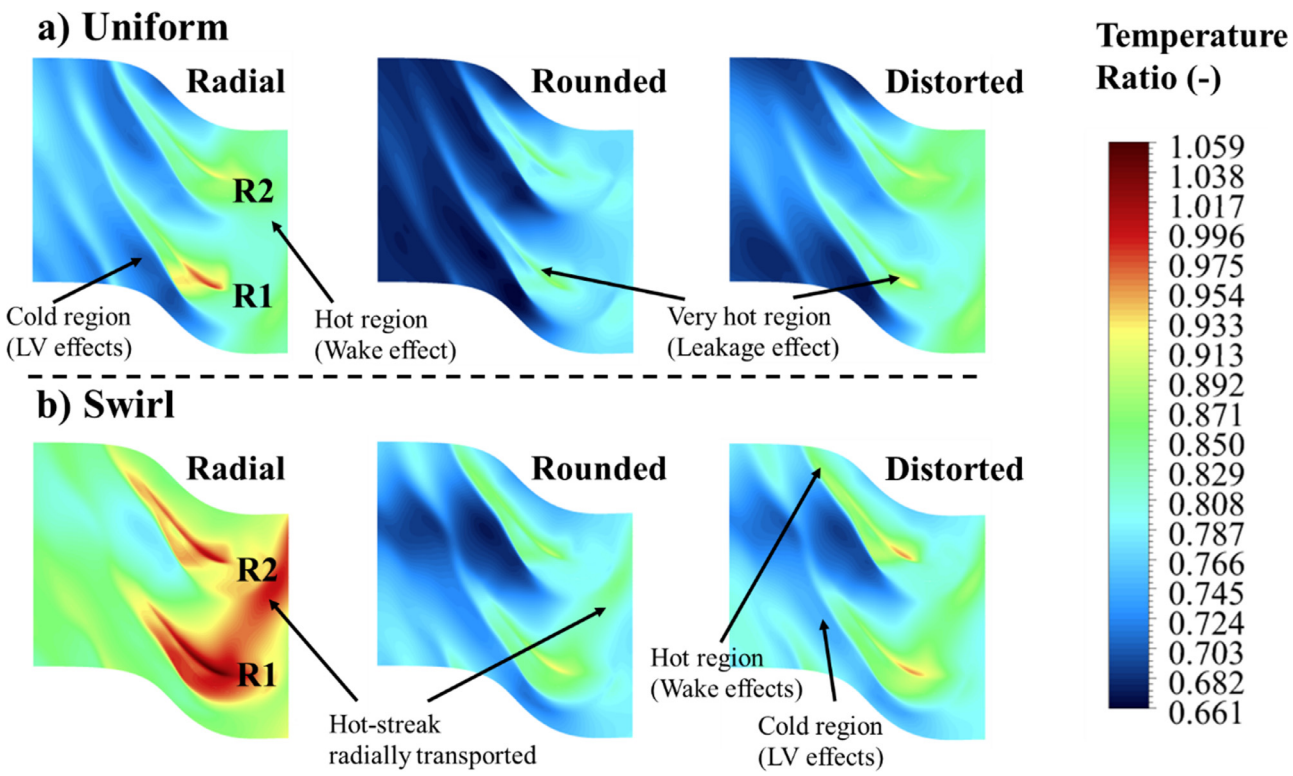


**Fig. 12.** Instantaneous static temperature ratio contours on the shroud under uniform and swirl conditions.

served for the "Distorted" case and it takes the value of 0.7%. At the tip surface, the effect of the swirl is clearly remarkable. As the inlet swirl is introduced, a significant increase in the average temperature takes place, for all hot-streaks. The increases are 5.9%, 6.68% and 4.79% for the "Radial", "Rounded" and "Distorted" cases, respectively with respect to the uniform case. It can be seen that the mixing induced by the residual swirl has its highest impact on the "Rounded" case and lowest impact on the "Distorted" case.

### 4.3. Endwall surface temperature

Fig. 12 depicts instantaneous static temperature ratio contours on the shroud surface under both axial flow and residual swirl inlet conditions. Generally, at both inflow conditions, the shroud inlet features the highest temperature due to the hot-streak and the shroud mid-region above the blade tip exhibits the harshest thermal load due to the hot leakage flow effects. This mid-region already suffers from the compressibility effects and shock formation due to the high speed of the tip and the tight gap, as previously reported [15]. The shock may increase the flow temperature and this is combined with both the shroud inlet hot-flow and hot leakage flow, which leads to temperature ratios above 1. The downstream region features the lowest temperature due to the LV effects. It was shown above that the LV is hot and that it drives the hot flow away from the shroud to allow colder flow to be in contact with the shroud. Particularly, with swirl conditions (Fig. 11(a)), the temperature map changes significantly and the transported hot-streak from the vane is clearly visible on the shroud. It was previously shown in (Fig. 8) that the swirl induces a deformation and radial distribution of the hot-streak from the hub to the shroud. The deformed hot-streak migrates towards the first blade rotor R1 and it impinges mainly onto the PS region. This behaviour is clearly visible for the "Radial" case in Fig. 12(a) due to the strong temperature gradient compared with the other cases. It can also be seen that the wake from the second rotor R2 generates a hot flow whereas the R1 wake has a cold flow.

Fig. 13 shows static temperature ratio maps on the hub surface under both axial flow and residual swirl inlet conditions. Before discussing the effect of the residual swirl on the different hot-streaks at the hub surface, it is important to mention some flow features on the rotor hub. It was found previously [15] that the hub region features two three secondary flows, which are the passage vortex, the horse-shoe vortex (HSV) and the corner vortex (CV). The PV is formed on the SS near the maximum camber region and it propagates downstream of the blade. The HSV is formed near the blade LE due to the mainstream and blade LE interaction. The CV is formed in the blade-hub junction near the mid-chord region at the PS and transported to just upstream of the stage exit. With uniform conditions (Fig. 13(a)), the HSV features a low temperature because the hot-streak is mainly located around the midspan region. From the mid-chord region to the downstream region, the LV and CV play an important role in enhancing mixing between the hot-streak and cold flow near the hub. The mixing effect by these secondary flows is significant for the "Radial" and "Distorted" case and it is very weak for the "Rounded" case. This is because the "Rounded" hot-streak has the lowest hot fluid area compared to the other hot-streaks. Thus, the secondary flows interact very weakly with this hot-streak and mixing does not occur. With swirl conditions (Fig. 13(b)), the hub temperature distribution changes remarkably since the swirl induces more mixing in this region. Both "Radial" and "Distorted" cases exhibit a drastic increase of the temperature due to the radial transport of the hot-streak. The "Radial" case is subject to the harshest thermal load among the others because the initial endwall cooling film is transported towards the midspan region and it is replaced by very hot flow from the hot-streak centre. It is clearly seen that the HSV of the first rotor features low temperature compared to the HSV of the second rotor. This is also due to the deformation of the hot-streak. The "Rounded" case, it exhibits the lowest thermal load among

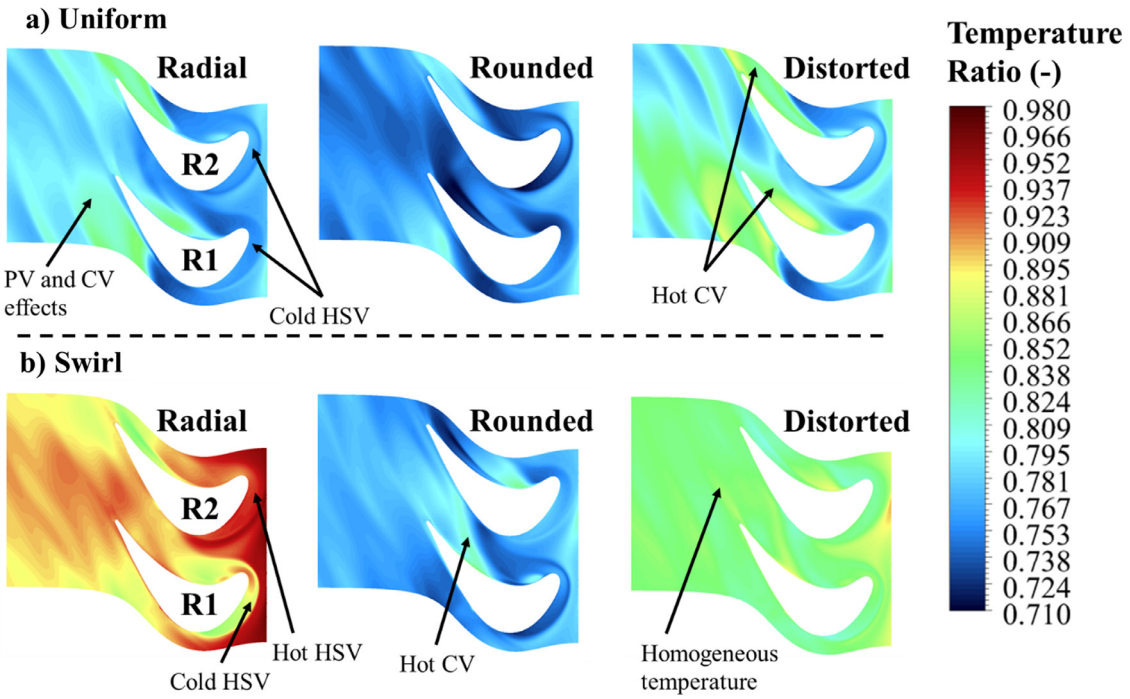


**Fig. 13.** Instantaneous static temperature ratio contours on the hub under uniform and residual swirl conditions.

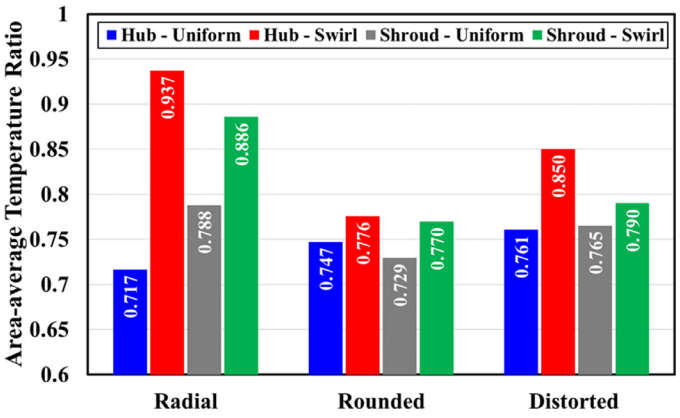


**Fig. 14.** Area-averaged static temperature of the shroud and hub surfaces for all the investigated cases.

the other hot-streaks and only a small hot temperature region appears owing to the effect of the CV. The "Distorted" case features a medium thermal load with almost homogeneous temperature on its entire surface.

To provide an appropriate quantitative analysis of the thermal load on the endwall surfaces, the area-averaged static temperature for each hot-streak under both uniform and swirl conditions is plotted in Fig. 14. For the shroud surface, the residual swirl has an important impact on the "Radial" case and lower impact on the other case. It increased the surface temperature by 23.48%, 5.32% and 3.16% for the "Radial", "Rounded" and "Distorted" cases, respectively with regards to the uniform condition. At the hub surface, it can be seen that the residual swirl has a stronger impact than its previous impact on the shroud. The "Radial" and "Distorted" cases are most affected by the swirl mixing. The temperature of the "Radial" and "Distorted" case is increased by 11.06% and 10.47%, respectively with regards to the uniform case. The impact on the average temperature of the "Rounded" case is lower and it is of 3.73%. It can be concluded that the hub is the surface that suffers most from the harshest thermal load compared to the other surfaces (i.e., the blade, the tip and the shroud).

### 4.4. Rotor heat transfer

Fig. 15 shows heat transfer coefficient distributions on the first rotor blade R1 surface at the tip and SS regions. It is important to note that the HTC evaluation requires two separate calculations. The first one is with an adiabatic wall condition, which allows the prediction of the surface temperature during the iterative solution. Consequently, the solver cannot predict the HTC since the wall heat flux is zero. The second calculation is based on a thermal law-of-the-wall, and it is defined as follows:

$$HTC = \frac{\rho c_p v^*}{T^+} \tag{3}$$

where $\rho$ is the density of the air, $c_p$ is the heat capacity of the air, $v^*$ is the velocity scale in the logarithmic part of the boundary layer and $T^+$ is a normalized temperature near the wall. The detailed definitions of the velocity scale and normalized temperature depend on the type of the turbulence model used and can be found in [38]. But in general, the velocity scale is calculated based on the turbulent model constant ($C_\mu$) and turbulence kinetic energy ($k$). The normalized temperature is calculated based on the Prandtl number ($P_r$) and dimensionless near wall grid distance ($y^*$). Thus, the upper term can be considered as a viscous term and the lower term as a thermal term.

It can be seen that the highest HTC regions are on the tip surface and rotor blade SS near the tip for all the investigated hot-streaks. This is obvious due to the leakage flow when it crosses the tip gap region and then forms the LV. During this process, the leakage generates high shear tress ($\tau$) due to the tight space and high flow speed. This $\tau$ is proportional to the turbulence kinetic energy and it is known that higher $\tau$ leads to higher $k$. Consequently, the significant local rise of $k$ impacts directly the viscous term (Eq. 3) to be much more significant than the thermal term and then the HTC increases. Regarding the effect of residual swirl, it can be seen that it contributes to the increase of the HTC on the rotor SS (red

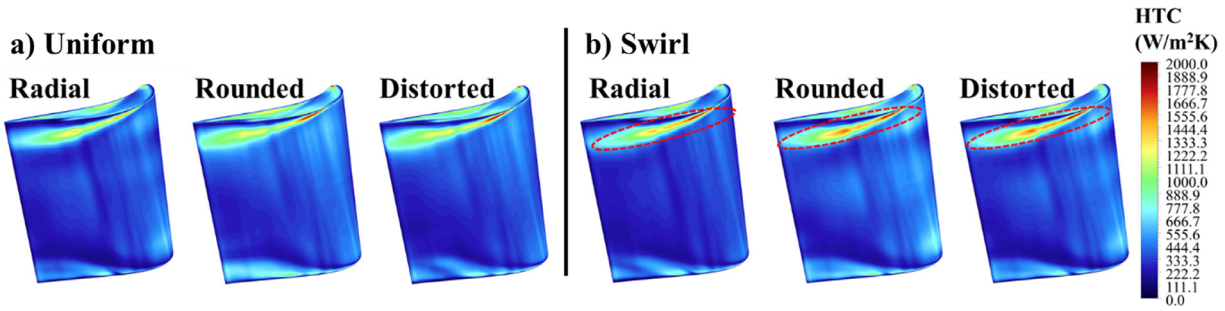


**Fig. 15.** Instantaneous surface heat transfer coefficient of the rotor blade tip and SS for all the investigated hot-streaks: (a) with uniform inlet flow and (b) with inlet swirl condition.

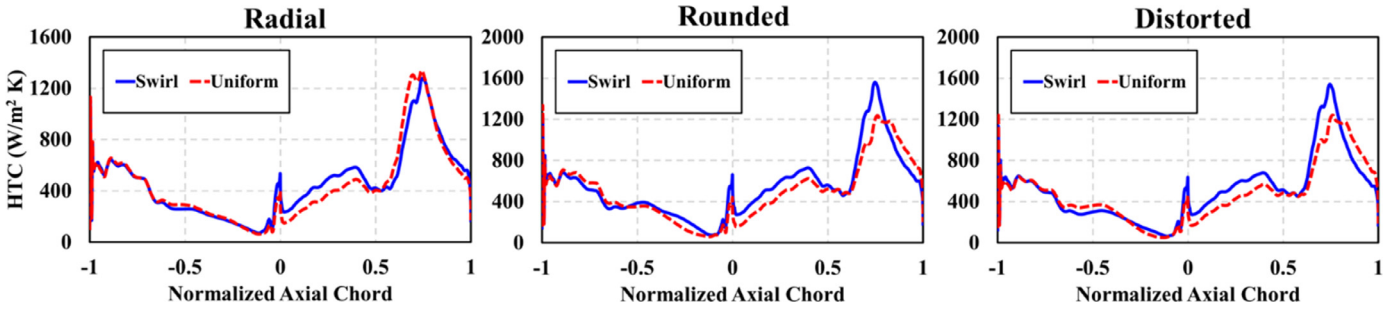


**Fig. 16.** Surface heat transfer coefficient of the rotor blade PS and SS for all the investigated hot-streaks: (a) with uniform inlet flow and (b) with inlet swirl condition.

dashed line in Fig. 14(b)) as expected. The flow rotation induces higher shear stress and this intensifies the LVs to have more kinetic energy and as a result higher HTC. Furthermore, the HTC near the hub is about 2.5 orders of magnitude lower than the HTC near the tip. This indicates that the hub secondary flow (i.e. passage vortex) has less turbulent kinetic energy that produces lower HTC.

To provide an insightful quantitative analysis of the thermal characteristic near the rotor tip region, the profiles of HTC at 90% blade span are plotted in Fig. 16. Negative values of the normalized axial chord distance ($C_{ax}$) indicate the blade PS and positive values of the normalized axial chord distance indicate the blade SS. In general, the HTC distribution at this location has almost the same trend for all the cases. It is important to note that the investigated rotor blade is a subject of boundary layer transition at both the SS and PS as reported in [10]. Boundary layer transition on the PS occurs at about the first chordwise half of the blade downstream of the LE ($0 > C_{ax} > -0.5$). The transition happens when the stagnating flow on the LE reaccelerates again and the highly cambered shape of the PS causes an over-acceleration that forms a laminar recirculation bubble across the whole span. Similar separation bubble was identified experimentally by Hodson and Dominy [44]. At this location, HTC reaches its lowest values of around 59 W/m$^2$ K. Downstream the mid-chord region ($C_{ax} < -0.5$), the boundary layer is fully turbulent and the HTC increases progressively till its maximum value of around 669 W/m$^2$ K at $C_{ax}$=-0.88 for all the cases. At the SS, the blade exhibits another boundary layer transition and this time is due to the presence of a shock that induces a separation and re-attachment of the boundary layer after forming a laminar bubble. This strong interaction reduces significantly the HTC, for example, for the "Radial" case at uniform flow the HTC decreased from 491 W/m$^2$ K at $C_{ax}$=0.4 to 403 W/m$^2$ K at $C_{ax}$=0.53. Downstream of the shock region ($C_{ax} \sim 0.5$), the boundary layer is subjected to relaxation and reacceleration to be fully turbulent and it interacts with the LV to generate higher heat transfer rates that reach a peak of 1330 W/m$^2$ K at $C_{ax}$=0.74 for the "Radial" case at uniform flow as an example. Moreover, the introduction of the residual swirl intensifies the heat transfer on the SS region for all the hot-streaks. For example, the HTC peak around the location $C_{ax}$=0.75 is increased by 22.43% and 19.3% for the "Rounded" and "Distorted" cases, respectively with regard to the non-swirl condition. The HTC peak of the "Radial" case does not exhibit a change under the residual swirl and this just a local behaviour at 90% span. At higher span values (>90%), closer to the tip the swirl obviously intensifies the HTC of all the cases including the "Radial" one as previously shown in Fig. 15(b).

## 5. Conclusion

A model turbofan high-pressure turbine stage has been investigated under combined residual swirl and hot-streak effects. Three hot-streak topologies were examined, which are an ideal "Radial" hot-streak that comprises a hot temperature gradient with film cooling effects near the endwalls. An ideal "Rounded" hot-streak that has a centred circular hot core surrounded by relatively cold temperature. A "Distorted" hot-streak features a large deformed hot core connected to a hot strip and it was generated from a lean burn combustor simulator of modern aero-engines. Investigations were conducted using unsteady Reynolds-averaged Navier–Stokes (URANS) computations. To the authors' knowledge, this study is the first computational investigation that compares results of the effects of representative lean burn combustor hot-streak and ideal hot-streaks from the literature (radial and rounded) combined with residual swirl on the aerothermal performance of a rotating turbine stage.

As the hot-streak is transported axially under uniform flow condition it was almost preserved downstream of the vane and remarkably altered through the rotor under the secondary flows effects. At the stage exit, the high temperature region within the hot-streak remained at the mid-passage zone for each hot-streak type but it underwent a roll-up deformation. These results support the conclusions of previous research regarding the higher effects of the rotor in modifying the hot-streak topology compared

to the vane effects. When the residual swirl is introduced, all hot-streaks were altered through the vane and deformed more through the rotor passage. The swirl motion has introduced a mixing of the flow from the stage inlet to its exit. The stage exit flow was characterized by a homogenised temperature distribution for the "Radial" case and dispersed hot-spots for the "Rounded" and "Distorted" cases. However, the temperature distribution of the "Distorted" case through the rotor was found to be the most complex among the other ideal hot-streaks.

The rotor blade surface temperature was highly affected by the hot-streak type and flow inlet conditions. Under "Radial" hot-streak, the whole rotor surfaces suffered from high levels of temperature because of the simplified topology of the hot-streak that contains 80% by surface of hot fluid. Under "Rounded" and "Distorted" hot-streaks with uniform flow, the rotor faced high levels of temperature around the midspan regions. It was expected that the hot-streak will be printed on this region under such axial transport effect. In addition, the near endwall regions including the tip surface were found with relatively low temperature. When the inlet swirl is combined with the "Rounded" and "Distorted" hot-streak, the midspan regions no longer suffer from very hot temperatures but the hot-streaks are spread almost all over the span near the rotor trailing edge. On the tip surface, the mid chord region exhibits high temperatures levels compared to the uniform case due to the radial transport of the hot-streak.

For the thermal load on the endwalls, results showed that the secondary flows play an important role on affecting the surface temperature gradient on both the shroud and hub. The shroud inlet features high temperatures from the hot steaks and the downstream region features low temperatures due to the leakage vortex effects. This later drives the hot fluid from the shroud towards the midspan region. Under the residual swirl condition, the radial transport of hot-streak increases the thermal gradient on the shroud. The temperature ratio exceeds unity near the tip region due to the shock presence. The hub was found the surface which most suffers from the harshest thermal load compared to the other surfaces. The highest surface temperature increase was found for the "Radial" case.

Results of surface heat transfer coefficient on the rotor blades revealed that the tip surface and SS near tip region suffer from the highest heat transfer rates. It was found that the leakage flow induces high shear stress that contributes to intensifying the highest heat transfer rate around the tip region. The residual swirl was found to intensify the leakage flow and, in particular the leakage vortex and hence, the heat transfer rate increases around the tip region.

As a general conclusion, the results of the present study revealed that over-simplified hot-streak topologies similar to the "Radial" case generate non-realistic thermal behaviour with an excess of high temperature levels. A "Rounded" topology could be an alternative to the previous case to overcome the excess of high temperature levels. However, its simplified circular shape may not provide the full picture of the thermal behaviour of a turbine stage with all of its complexity. The "Distorted" hot-streak was found to generate a complex thermal behaviour through the turbine stage. Its transport and effect on the rotor surface were a changeling aspect to analyse.

## CRediT author statement

**Zakaria Mansouri:** Conceptualization, Methodology, Software, Validation, Formal analysis, Investigation, Writing - Original Draft, Writing - Review & Editing, Visualization, Project administration. **Richard Jefferson-Loveday:** Conceptualization, Supervision, Resources, Writing - Review & Editing, Project administration.

## Declaration of Competing Interest

The authors declare that they have no known competing financial interests or personal relationships that could have appeared to influence the work reported in this paper.

## References


[1] P. Gaetani, G. Persico, L. Pinelli, M. Marconcini, R. Pacciani, Computational and Experimental Study of Hot Streak Transport Within the First Stage of a Gas Turbine, ASME. J. Turbomach. 142 (8) (August 2020) 081002, doi:10.1115/1.4045961.

[2] M.G. Adams, T. Povey, B.F. Hall, D.N. Cardwell, K.S. Chana, P.F. Beard, Commissioning of a Combined Hot-Streak and Swirl Profile Generator in a Transonic Turbine Test Facility, ASME. J. Eng. Gas Turbines Power. 142 (3) (March 2020) 031008, doi:10.1115/1.4044224.

[3] A. Notaristefano, P. Gaetani, Impact of Swirling Entropy Waves on a High Pressure Turbine, ASME. J. Turbomach 144 (3) (March 2022) 031010, doi:10.1115/1.4052353.

[4] YANG Xing, HAO Zihan, FENG Zhenping, Particle deposition patterns on high-pressure turbine vanes with aggressive inlet swirl, Chin. J. Aeronaut. 35 (3) (2022) 75–89 VolumeIssuePages, doi:10.1016/j.cja.2021.06.005.

[5] B. Martin, F. Duchaine, L. Gicquel, N. Odier, J. Dombard, Accurate Inlet Boundary Conditions to Capture Combustion Chamber and Turbine Coupling With Large-Eddy Simulation, ASME. J. Eng. Gas Turbines Power 144 (2) (February 2022) 021007, doi:10.1115/1.4052099.

[6] TIP Shih, YL. Lin, Controlling secondary-flow structure by leading-edge airfoil fillet and inlet swirl to reduce aerodynamic loss and surface heat transfer, J. Turbomach. 125 (1) (2003) 48–56.

[7] M.I. Qureshi, T. Povey, A Combustor-Representative Swirl Simulator for a Transonic Turbine Research Facility, Proc. Inst. Mech. Eng., Part G 225 (7) (2011) 737–748.

[8] I. Qureshi, A.D. Smith, T. Povey, HP Vane Aerodynamics and Heat Transfer in the Presence of Aggressive Inlet Swirl, ASME J. Turbomach. 135 (2) (2013) 021040.

[9] I. Qureshi, A. Beretta, K. Chana, T. Povey, Effect of aggressive inlet swirl on heat transfer and aerodynamics in an unshrouded transonic HP turbine, J. Turbomach. 134 (6) (2012) 061023.

[10] G Schmid, HP. Schiffer, Numerical investigation of inlet swirl in a turbine cascade, ASME, New York, 2012 Report No.: GT2012-69397.

[11] T Povey, KS Chana, TV Jones, et al., The effect of hot-streaks on HP vane surface and endwall heat transfer: An experimental and numerical study, J. Turbomach. 129 (1) (2007) 32–43.

[12] CI Smith, D Chang, S Tavoularis, Effect of Inlet Temperature Non-Uniformity on High-Pressure Turbine Performance, in: Proceedings of the ASME Turbo Expo 2010: Power for Land, Sea, and Air. Volume 7: Turbomachinery, Parts A, B, and C. Glasgow, UK. June 14–18, 2010, pp. 2465–2476.

[13] S Salvadori, F Montomoli, F Martelli, et al., Analysis on the effect of a nonuniform inlet profile on heat transfer and fluid flow in turbine stages, J. Turbomach. 134 (1) (2012) 011012.

[14] ZD Wang, ZF Liu, ZP. Feng, Influence of mainstream turbulence intensity on heat transfer characteristics of a high pressure turbine stage with inlet hot streak, J. Turbomach. 138 (4) (2016) 041005.

[15] Zakaria Mansouri, Unsteady simulation of flow and heat transfer in a transonic turbine stage under non-uniform inlet conditions, Int. Commun. Heat Mass Transfer 129 (2021) 105660 Volume.

[16] Zhiduo Wang, Dian Wang, Zhaofang Liu, Zhenping Feng, Numerical analysis on effects of inlet pressure and temperature non-uniformities on aero-thermal performance of a HP turbine, Int. J. Heat Mass Transfer 104 (2017) 83–97 VolumePages.

[17] S. Luque, V. Kanjirakkad, I. Aslanidou, R. Lubbock, B. Rosic, S. Uchida, A New Experimental Facility to Investigate Combustor–Turbine Interactions in Gas Turbines With Multiple Can Combustors, ASME. J. Eng. Gas Turbines Power. 137 (5) (May 2015) 051503.

[18] Z. Mansouri, R. Belamadi, The influence of inlet swirl intensity and hot-streak on aerodynamics and thermal characteristics of a high pressure turbine vane, Chinese J. Aeronaut 34 (2021) 66–78.

[19] D. Griffini, M. Insinna, S. Salvadori, F. Martelli, Clocking Effects of Inlet Nonuniformities in a Fully Cooled High-Pressure Vane: A Conjugate Heat Transfer Analysis, ASME. J. Turbomach 138 (2) (February 2016) 021006.

[20] D Charbonnier, P Ott, M Jonsson, T Ko¨bke, F. Cottier, Comparison of Numerical Investigations With Measured Heat Transfer Performance of a Film Cooled Turbine Vane, in: Proceedings of the ASME Turbo Expo 2008: Power for Land, Sea, and Air. Volume 4: Heat Transfer, Parts A and B. Berlin, Germany. June 9–13, 2008, pp. 571–582.

[21] A Andreini, T Bacci, M Insinna, L Mazzei, S. Salvadori, Modelling strategies for the prediction of hot streak generation in lean burn aeroengine combustors, Aerosp. Sci. Technol. 79 (2018) 266–277.

[22] Zhiduo Wang, Dian Wang, Zhihao Wang, Zhenping Feng, Heat transfer analyses of film-cooled HP turbine vane considering effects of swirl and hot streak, Appl. Therm. Eng. 142 (2018) 815–829 VolumePages.

[23] Z. Mansouri, Numerical prediction of heat transfer characteristics on a turbine nozzle guide vane under various combustor exit hot-streaks, Heat. Transf 51 (2022) 976–997.

[24] C Koupper, G Bonneau, L Gicquel, F Duchaine, Large Eddy Simulations of the Combustor Turbine Interface: Study of the Potential and Clocking Effects, in: *Proceedings of the ASME Turbo Expo 2016: Turbomachinery Technical Conference and Exposition*. Seoul, South Korea. June 13–17, 2016.
[25] Wenhao Zhang, Zhiduo Wang, Zhihao Wang, Ruocheng Li, Zhenping Feng, Study on heat transfer characteristics of NGVs influenced by non-reacting lean burn combustor simulator flow, Int. J. Therm. Sci. 172 (2022) 107313 VolumePart A.
[26] Jingyu Wang, Ning Ge, Chunhua Sheng, Analysis of swirling flow effects on the characteristics of unsteady hot-streak migration, Chin. J. Aeronaut. 29 (6) (2016) 1469–1476 VolumeIssuePages.
[27] B. Khanal, L. He, J. Northall, P. Adami, Analysis of radial migration of hot-streak in swirling flow through high-pressure turbine stage, J. Turbomach 135 (2013) 041005.
[28] A. Rahim, L. He, Rotor blade heat transfer of high pressure turbine stage under inlet hot-streak and swirl, J. Eng. Gas Turbines Power 137 (2015) 062601.
[29] Z. Liu, Z. Wang, Z. Feng, Effects of inlet swirl on hot streak migration across tip clearance and heat transfer on rotor blade tip, in: *Proc. ASME Turbo Expo*, Montreal, Canada, 2015.
[30] Zhihao Wang, Zhiduo Wang, Wenhao Zhang, Zhenping Feng, Numerical study on unsteady film cooling performance of turbine rotor considering influences of inlet non-uniformities and upstream coolant, Aerosp. Sci. Technol. 119 (2021) 107089 Volume.
[31] M.G. Adams, P.F. Beard, M.R. Stokes, F. Wallin, K.S. Chana, T. Povey, Effect of a combined hot-streak and swirl profile on cooled 1.5-stage turbine aerodynamics: an experimental and computational study, J. Turbomach 143 (2021) 021011.
[32] LJ Goldman, KL. McLallin, Cold air annular cascade investigations of aerodynamic performance of core-engine- cooled turbine vanes. 1: Solid vane performance and facility description, Washington, D.C.: NASA (1975) Report No.: NASA TM X-3224.
[33] Zakaria Mansouri, Abdelhakim Settar, Hamza Khamane, Computational investigation of heat load and secondary flows near tip region in a transonic turbine rotor with moving shroud, Appl. Therm. Eng. (136) (2018) 141–151 VolumePages.
[34] Zakaria Mansouri, Aerodynamic and heat transfer performances of a highly loaded transonic turbine rotor with upstream generic rim seal cavity, Propulsion and Power Research 10 (4) (2021) 317–331 VolumeIssuePages.
[35] T. Arts, J.Rollin. J-M.Duboué, Aerothermal Performance Measurements and Analysis of a Two-Dimensional High Turning Rotor Blade, Trans. ASME 120 (1998) 494–499.
[36] F.R. Menter, Two-equation eddy-viscosity turbulence models for engineering applications, AIAA J. 32 (1994) 1598–1605.
[37] R.B. Langtry, F.R. Menter, Correlation-Based Transition Modeling for Unstructured Parallelized Computational Fluid Dynamics Codes, AIAA J. 47 (12) (December 2009) 2894–2906.
[38] ANSYS Inc.ANSYS CFX-solver theory guide, ANSYS Inc., Canonsburg, 2019.
[39] M.H. Rahman, S.I. Kim, I. Hassan, Effects of Inlet Temperature Uniformity and Nonuniformity on the Tip Leakage Flow and Rotor Blade Tip and Casing Heat Transfer Characteristics, ASME. J. Turbomach. March 2012; 134 (2) (June 21, 2011) 021001.
[40] P. Malan, K. Suluksna, E. Juntasaro, Calibrating the Gamma-Re_theta Transition Model for Commercial CFD, 47th AIAA Aerospace Sciences Meeting including The New Horizons Forum and Aerospace Exposition. 47th AIAA Aerospace Sciences Meeting including The New Horizons Forum and Aerospace Exposition, American Institute of Aeronautics and Astronautics, 2009, doi:10.2514/6.2009-1142.
[41] S. Mauro, R. Lanzafame, M. Messina, D. Pirrello, Transition turbulence model calibration for wind turbine airfoil characterization through the use of a Micro-Genetic Algorithm, In International Journal of Energy and Environmental Engineering 8 (4) (2017) 359–374 Vol.Issue.
[42] Z Mansouri, T Boushaki, M. Aouissi, Detached eddy simulation of non-reacting swirling flow in a vortex burner, Int. J. Heat Technol. 35 (2017) 594–602.
[43] Z Mansouri, T. Boushaki, Investigation of large-scale structures of annular swirling jet in a non-premixed burner using delayed detached eddy simulation, Int. J. Heat Fluid Flow 77 (2019) 217–231.
[44] H.P. Hodson, R.G. Dominy, Three-Dimensional flow in a Low-Pressure Turbine Cascade at Its Design Condition, ASME Tran. J. Turbomachinery 109 (1987) 177–185.
[45] Adel Ghenaiet, Kaddour Touil, Characterization of component interactions in two-stage axial turbine, Chin. J. Aeronaut. 29 (4) (2016) 893–913 VolumeIssuePages.
[46] Joshua Horwood, PhD Thesis, University of Bath, 2019.
[47] Nicolas Gourdain, Prediction of the unsteady turbulent flow in an axial compressor stage. Part 2: Analysis of unsteady RANS and LES data, Comput. Fluids (106) (2015) 67–78 VolumePages.